Local atomic structure of semiconductor alloys using pair distribution functions. II.

Jean S. Chung
Department of Physics, Chungbuk National University, Cheongju, Chungbuk, 361-763, Republic of Korea

M. F. Thorpe
Department of Physics and Astronomy and Center for Fundamental Materials Research, Michigan State University, East Lansing, Michigan 48824

(Received 8 July 1998)

A method of calculating the pair distribution function in semiconductor alloys has been extended to the differential and the partial pair distribution functions, and applied to pseudobinaries of the form $A_{1-x}B_xC$ with the zinc-blende structure. We have used a simple valence force model with bond-stretching and bond-bending forces. Results of calculations are presented for $Ga_{0.5}In_{0.5}As$. The differential pair distribution function provides a useful experimental way of determining the structural distortions in semiconductor alloys—specifically the mean nearest-neighbor and second-neighbor distances and widths can be obtained for chemically specific pairs of atoms. [S0163-1829(99)00407-5]

I. INTRODUCTION

Semiconductor alloys have received much attention because physical properties, such as the band gap, mobility, and lattice parameter, can be continuously controlled by varying the chemical composition. Having such continuous controls is of importance in applications such as electronic and optical devices.[1] Local structural information is important in understanding most physical properties of the alloy. However, the structural characterization of alloys is not trivial, because the internal strain induced by the bond-length mismatch between different chemical species, which causes complex local strain patterns, complicates the situation.

Besides the bond-length mismatch, there are different kinds of pairs in alloys, and even the same kinds of pairs have different *local* environments. For example, in the pseudobinary alloy $Ga_{1-x}In_xAs$, there are *two* different types of nearest-neighbor pairs (In-As and Ga-As) and *five* different types of next nearest neighbor pairs In-As-In, Ga-As-Ga, In-As-Ga, As-In-As and As-Ga-As, each of which has different local surroundings. Therefore, studying local atomic structures will require quite an effort to sort out experimentally. The experimental characterization of alloys has relied mainly upon two methods. Bragg diffraction methods have measured the structural quantities that are correlated over *long* distances such as the lattice constant, while extended x-ray absorption fine-structure (XAFS) experiments have provided the *short*-distance information such as the near-neighbor distances. The mean nearest-neighbor distances for each of the two kinds of pairs can be obtained by XAFS in most cases,[2] but the five mean second-neighbor distances have been obtained in only one case that we are aware of.[3] Thus having an alternative approach that allows the mean lengths to be obtained, and in addition the widths, is very desirable. Diffraction experiments always have the advantage over XAFS, that the interpretation is more straightforward. Recently, synchrotron x-ray sources and spallation neutron sources have made high-momentum scattering data available. The diffuse background in diffraction experiments is now utilized to extract the *short*- to *intermediate*-distance information using pair distribution function (PDF) analysis.[4] The PDF, which represents the probability of finding an atom, consists of series of peaks as a function of the separation.

In our previous work,[5] henceforth referred to as paper I, we developed a method of calculating the PDF of binary semiconductor crystals with the zinc-blende structure AC and the associated pseudobinary random alloys, $A_{1-x}B_xC$. We used a harmonic valence bond model,[6] which had been successful in describing the local strain in semiconductor alloys, and incorporated the thermal motion of atoms quantum mechanically. The results of calculations using this method compared nicely with the first preliminary experiments,[7] which demonstrated the feasibility of the method. We showed that the nearest-neighbor peak has a double-peak substructure at low temperatures because the length distributions of two different types of pairs are sufficiently separated. This substructure can therefore be resolved experimentally if the experiment is done at a sufficiently low temperature. The *widths* of the these nearest-neighbor peaks can also be extracted. On the other hand, the substructure in the next-nearest-neighbor peak cannot be observed in the PDF, even at the lowest temperatures, because the different types of pairs have almost overlapping length distributions, which are further mixed together into a single peak in the PDF by the zero point motion.[5]

Even after the above considerations, there is still another experimental complication. Scattering data can be obtained only up to a finite value of the momentum transfer $q_{\max}$. In order to obtain the PDF, therefore, the data should be convoluted with a step function, the width of which is given by $q_{\max}$. The convolution integral tends to further blur sharp structures and produces ripples around PDF peaks, deteriorating the quality of the PDF,[5] and hence makes interpretation very difficult or impossible.

The degree of this degradation depends upon the value of $q_{\max}$, as shown in the example in Fig. 1. Only the top two curves, (*a*) and (*b*), corresponding to $q_{\max}=50$ and 40 Å^{-1},

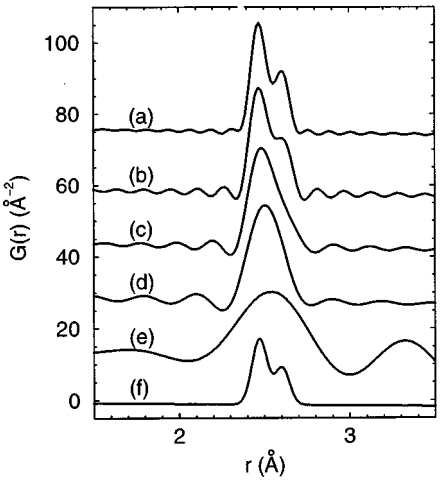

FIG. 1. The convoluted PDF's of $Ga_{0.5}In_{0.5}As$ with q_{max} values of (*a*) 50, (*b*) 40, (*c*) 30, (*d*) 20, and (*e*) 10 Å^{-1} are compared with (*f*) the unconvoluted theoretical PDF. Curves are calculated for neutron scattering at $T=10$ K. Curves $(a)-(e)$ are shifted upward for clarity. It can be seen that the double-peak substructure in the nearest-neighbor peak can be resolved only with higher values of q_{max}.

can resolve the double-peak structure of the *true* curve at the bottom (*f*), which is theoretically calculated with $q_{max}=\infty$. This kind of q_{max} can now be achieved with synchrotron sources. Even with $q_{max}=30$ Å^{-1}, which is beyond the limit of conventional x-ray sources, the substructure of the peak disappears. At the lowest q_{max} in the figure, the ripples can be of a comparable size with the peak itself. At high temperatures, the situation becomes worse since the double peak merges into one, even in theoretical calculations, with $q_{max}=\infty$, due to thermal fluctuations.

The layout of this paper is as follows. In the next section, we define the differential and partial PDF's. We closely follow the procedure developed in paper I, which should be read before this paper. We suggest that measuring these quantities can solve some of the experimental and interpretation problems mentioned above. Of course, the differential and partial PDF's provide more information than the total PDF, and we show they can resolve the substructure in the nearest-neighbor peak under most experimental conditions, and can do so in the next-nearest-neighbor peak under certain conditions.

II. PAIR DISTRIBUTION FUNCTION

In this section, we briefly discuss various definitions used in this paper. Note that we adopt a different nomenclature from that of paper I, which seems more consistent with the broader body of literature,[8] and we will make notes of the specific changes as they occur.

For the sake of simplicity, we begin with an arrangement of N identical atoms.[4] Let us denote the position of the ith atom as $\mathbf{r}_i$ and define $\mathbf{r}_{ij}=\mathbf{r}_j-\mathbf{r}_i$, which is a vector from the atom i to j. The probability density of finding the pair ij at the position $\mathbf{r}$ is given by

$$\rho_{ij}(\mathbf{r})=\langle\delta(\mathbf{r}-\mathbf{r}_{ij})\rangle, \tag{1}$$

where $\langle\cdots\rangle$ denotes the statistical average that implies *both* configurational and thermal averages. This function is summed over all pairs and further averaged by taking each atom in turn as the origin to give the *density function* (this was referred as the pair distribution function in paper I):

$$\rho(r)=\frac{1}{N}\sum_i{\sum_j}' \rho_{ij}(\mathbf{r}), \tag{2}$$

where the prime in the summation means that the terms $i=j$ are excluded. The density function (2) describes the average probability per unit volume of finding an atom at a position $\mathbf{r}$ from an atom at the origin. It converges to unity at large distance in most materials.

In this study, the major interest lies in macroscopically *isotropic* materials, such as pure randomly oriented crystallites. In such materials, the probability of finding pairs depends only on the magnitude r. For isotropic materials, it is often convenient to define the one-dimensional probability density, namely, the *radial distribution function* (RDF) as $J(r)=4\pi r^2\rho(r)$, where $\rho(r)$ is the spherical average of the function $\rho(\mathbf{r})$. This probability should be interpreted as per unit length rather than per unit volume. The average number of atoms in a shell with radius r and thickness dr is given by $J(r)dr$. For ideally rigid and perfect crystals, the RDF consists of a series of δ function peaks with the weight given by the total number of atoms at that distance. In real crystals, however, the peaks are broadened by lattice imperfections and by the thermal motions of the atoms.

The RDF tends to obscure the correlations between atoms as r becomes larger because it grows rapidly as $\sim r^2$. Hence, it is customary to define the PDF (this was referred as the reduced RDF in paper I) as

$$G(r)=4\pi r[\rho(r)-\rho_0]=\frac{1}{r}[J(r)-4\pi r^2\rho_0], \tag{3}$$

where ρ_0 is the average *number* density of the material. Since the average density is subtracted, $G(r)$ oscillates around zero and shows the correlations more clearly than does the RDF.

Usually, it is the PDF to which the experimental diffraction data are transformed through the relation

$$G(r)=\frac{2}{\pi}\int_0^\infty F(q)\sin qr\,dq. \tag{4}$$

Here q is the magnitude of the scattering vector and $F(q)$ is the reduced scattering intensity defined by

$$F(q)\equiv q\left[\frac{I(q)}{Nf^2}-1\right], \tag{5}$$

where $I(q)$ is the experimentally measured scattering intensity. The quantity f is the (q-dependent) atomic form factor in x-ray scattering, and the (constant) scattering length in neutron scattering.

In the case of multicomponent systems,[4] the definition of the PDF is generalized to

$$\rho(\mathbf{r})=\frac{1}{N}\sum_i{\sum_j}' w_{ij}\rho_{ij}(\mathbf{r}). \tag{6}$$

Here, the relative weights w_{ij} are given by $f_i f_j/\overline{f}^2$, where f_i is the scattering strength of the atom i and $\overline{f}$ denotes the arithmetic mean of f_i's in the sample.

The system of interest in this study, $A_{1-x}B_xC$, can form six different types of pairs at any distance, namely, *A*-*A*, *A*-*B*, *B*-*B*, or *C*-*C* pairs between atoms in the *same* sublattice, and *A*-*C* or *B*-*C* pairs between atoms in *different* sublattices. Therefore, we define the (pair-specific) *partial density function* $\rho_{\mu\nu}$ (μ, $\nu=A$, *B*, or *C*) by Eq. (6) but with the sum restricted to the specified type of pair; that is either the ith atom is μ and the jth atom is ν, or vice versa. The (pair-specific) *partial PDF*, $G_{\mu\nu}$, can also be defined similarly using Eq. (3). These partial functions contain the information on the length distribution of the specific type of the pair in the alloy.

Another quantity of interest is the (atom-specific) *differential density function* ρ_μ and the (atom-specific) *differential PDF*, G_μ, where we restrict the sum so that either ith or jth atom is an atom of a specified chemical type. Then by definition

$$\rho_\mu=\sum_\nu \rho_{\mu\nu}. \tag{7}$$

These differential functions can be obtained in neutron scattering experiments by taking the difference of two PDF's from samples containing two different isotopes, or by working near an absorption edge with x rays.[8]

To proceed further, we rewrite $\rho_{ij}(r)$ as

$$\rho_{ij}(r)=\frac{1}{2\pi}\int dq e^{-iqr}\langle e^{iqr_{ij}}\rangle \tag{8}$$

and apply the harmonic approximation. This function would be a series of δ functions located at r_{ij} if all the atoms were stationary in a perfect crystal. However, this δ function is broadened by the *thermal motions* since the atoms move around the equilibrium positions even at zero temperature. The response is further broadened by the *internal strains* due to the bond-length mismatch in alloys.

Within the harmonic approximation, thermal averaging can be calculated using the Debye-Waller theorem. It has been shown in paper I that for a specific pair $\rho_{ij}(r)$ becomes *a Gaussian* peak centered at r_{ij} with the width σ_{ij} given by

$$\sigma_{ij}^2=\langle[\mathbf{u}_{ij}\cdot\hat{r}_{ij}]^2\rangle, \tag{9}$$

where $\mathbf{u}_{ij}=\mathbf{u}_j-\mathbf{u}_i$, and $\mathbf{u}_i$ is the displacement of the atom i, and $\hat{r}_{ij}$ is the unit vector in the direction of $\mathbf{r}_{ij}$. Therefore, the PDF consists of a series of Gaussians distributed over a length range determined by the local environment of each pair of atoms in the system.

Using of the quantum mechanical representation of the displacement, and thus rewriting u_{ij} in terms of phonon operators, it was shown in paper I that

$$\sigma_{ij}^2=\frac{2\hbar}{N}\sum_{k,s}\frac{1}{\omega_s(\mathbf{k})}(\langle n_{k,s}\rangle+\tfrac{1}{2})\times\left[\frac{|e_\mu(\mathbf{k},s)\cdot\hat{r}_{ij}|^2}{2M_\mu}+\frac{|e_\nu(\mathbf{k},s)\cdot\hat{r}_{ij}|^2}{2M_\nu}-\frac{|e_\mu(\mathbf{k},s)\cdot\hat{r}_{ij}||e_\nu(-\mathbf{k},s)\cdot\hat{r}_{ij}|e^{i\mathbf{k}\cdot\mathbf{r}_{ij}}}{\sqrt{M_\mu M_\nu}}\right], \tag{10}$$

where N is the number of Bravais lattice points, $\omega_s(\mathbf{k})$ is the eigenvalue of the dynamical matrix with the wave vector $\mathbf{k}$ in branch s, $\langle n_{k,s}\rangle$ is the number of thermally excited phonons, and $e_\mu(\mathbf{k},s)$ is the corresponding eigenvector associated with the basis μ and mass M_μ. The sum runs over the first Brillouin zone and also over all branches.

The PDF of the material can be calculated as follows: solving the eigenvalue problem of the dynamical matrix given by the model alloy with a particular configuration of atoms in a large supercell that is periodically repeated, one can calculate the width σ_{ij} by performing the sum (10) for *each individual pair* of atoms. Then the Gaussian located at r_{ij} with a calculated width σ_{ij} can be summed with the weight w_{ij} to give the particular PDF required. The actual distribution of r_{ij} can also be found from this approach. In the next section we give a number of examples of the results of this procedure.

The approach outlined here is quite general and does not rely on any particular potential. We have found the Kirkwood model adequate to date, but the procedure outlined here could be implemented with any potential.

III. CALCULATIONS

We consider a pseudobinary semiconductor alloy in the zinc-blende structure, $A_{1-x}B_xC$ with *A* and *B* atoms in one sublattice and *C* in the other. We adopt the Kirkwood model[9] for convenience as in paper I to account for the forces between the atoms in zinc-blende structures. The potential energy of this model is given by

$$V=\sum_{\langle i,j\rangle}\frac{\alpha_{ij}}{2}(L_{ij}-L_{ij}^0)^2+L_e^2\sum_{\langle ij,il\rangle}\frac{\beta_{ijl}}{8}(\cos\theta_{ijl}-\cos\theta^0)^2. \tag{11}$$

Here, the first term describes the energy due to the bond-stretching force with the force constant α_{ij} between atoms i and j. The lengths L_{ij} and L_{ij}^0 are the actual and natural (unstrained) bond lengths between the atoms i and j, respectively. The second term in Eq. (1) describes the bond-bending force with the force constant β_{ijl} between the bonds ij and il. The angles θ_{ijl} and θ^0 are the actual and natural (109.5°) angles between the bonds ij and il. The nearest-neighbor distance L_e as given by the virtual crystal approximation, is known to be exact[10] if there is no disorder in the force constants α and β as assumed here. The length L_e is

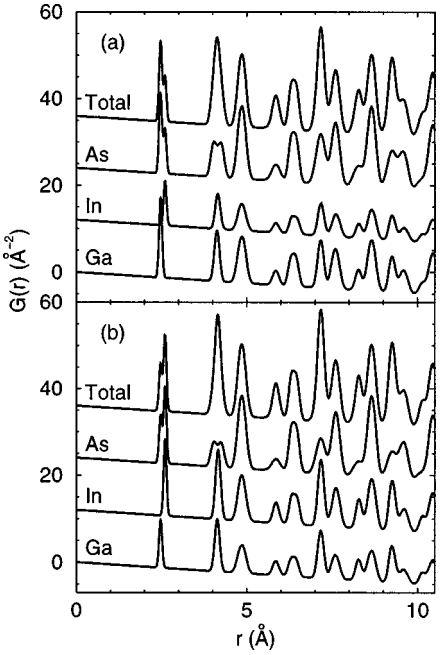

FIG. 2. The differential PDF's of $Ga_{0.5}In_{0.5}As$ for (a) neutron scattering and (b) x-ray scattering at $T=10\,K$ are compared with the total PDF. The top three curves are shifted upward in each panel for clarity.

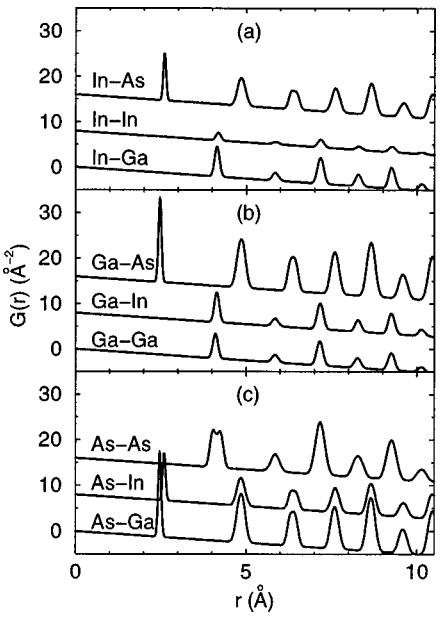

FIG. 3. The partial PDF's of $Ga_{0.5}In_{0.5}As$ associated with the (a) In, (b) Ga, and (c) As atoms for neutron scattering at $T=10\,K$. Adding the three curves in each panel gives the corresponding differential PDF's in Fig. 2(a). The top two curves are shifted upward in each panel for clarity.

inserted in the second term to make β_{ijl} have the same dimension as α_{ij}. The angular brackets under the summations denote counting each pair only once to exclude double counting. The potential (11) has been used extensively in discussing the elastic strain in semiconductor alloys.[6] We take $\alpha_{ij}=\alpha$ for *all* pairs and $\beta_{ijl}=\beta$ for *all* angles as in paper I.

To realize the alloy computationally, we employ the periodic supercell, which consists of $4\times4\times4$ cubic unit cells of $Ga_{0.5}In_{0.5}As$ containing 512 atoms. We have chosen this material because it has a large bond-length mismatch and forms a random solid solution. A configuration of the material is built by positioning In and Ga atoms randomly at the lattice points on one sublattice, the other sublattice always being occupied by As atoms. Then the system is relaxed using the conjugate gradient method to find the static equilibrium displacements. By solving the eigenvalue problem of the dynamical matrix numerically, the integration (10) can be performed to give σ_{ij} as described in paper I. Finally the appropriate PDF is calculated by adding Gaussians with the width given by σ_{ij} and the position given by the static relaxed structure. This whole procedure is iterated over different realizations of the supercell to perform a configurational average as needed.

The results of our theoretical calculations for the (atom-specific) differential PDF are depicted in Fig. 2. For the nearest neighbor peak near $r=2.5\,Å$, the As-related curve is the same as the total PDF since every nearest-neighbor peak has As atom at one end. However, the In-related and the Ga-related curves are specific to the In-As and the Ga-As bonds, respectively, and show the characteristic length of the corresponding bonds. Adding these two curves gives the total PDF. Note that, here and in the following, adding the differential or partial PDF's means the addition of the peaks only on the fixed baseline which decreases with r. The width of each peak is broader than the actual (static) bond length distribution because the PDF peaks are broadened by thermal motions. At 10 K, these thermal motions are mainly due to the zero point motion as shown in paper I.

For the next-nearest-neighbor peak near $r=4.2\,Å$, the As-related curve has the double-peak structure showing the characteristic lengths of the As-In-As and As-Ga-As local structures, while the In-related and the Ga-related curves occur at different positions showing the characteristic lengths of different local structures. In fact, the peak in the In-related curve comes from two types of pairs, In-As-In and In-As-Ga, and that in the Ga-related curve from Ga-As-In and Ga-As-Ga. Since the differences are so small, they appear as one peak. Although the double-peak structure of the As-related curve may not be resolved at higher temperatures due to thermal broadening, the difference in the In-related and the Ga-related curves may stay intact because thermal broadening does not change the peak positions. Addition of all three curves with appropriate weights gives the total PDF, which appears to be structureless because the three peaks are located very close to each other. Therefore, the differential PDF's can provide more information on the local structures than the total PDF, as expected, and this extra information is important.

The results of the theoretical calculations for the (bond-specific) partial PDF's are shown in Fig. 3, where adding all three curves in each panel of (a), (b), and (c) will give the corresponding curves in Fig. 2(a) for In-, Ga-, and As-related differential PDF's, respectively. Since the partial PDF is more restrictive in the sense that both end atoms of a pair should be of specific types, we have less intensity in each peak. We have a possibility of resolving the different types of pairs in the next-nearest pairs with the partial PDF's,

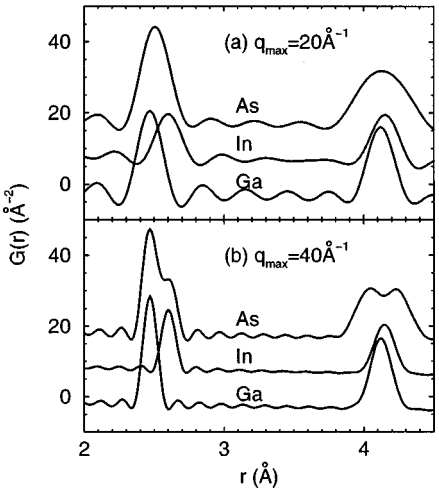

FIG. 4. The comparison of the neutron scattering differential PDF's of $Ga_{0.5}In_{0.5}As$ with different values of q_{max} at $T=10$ K. The curves are drawn for the first two neighbors and shifted upward for clarity.

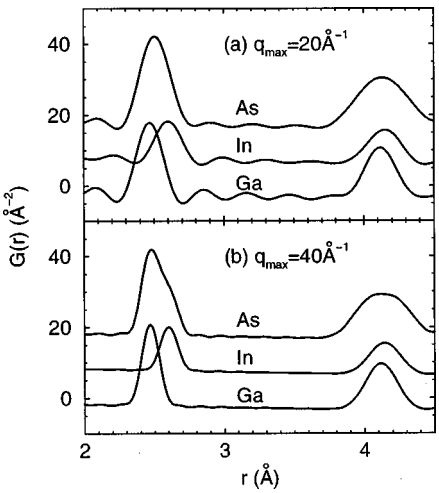

FIG. 5. The comparison of the neutron scattering differential PDF's of $Ga_{0.5}In_{0.5}As$ with different values of q_{max} at $T=300$ K. The curves are drawn for the first two neighbors and shifted upward for clarity.

which appeared as one peak in the differential PDF, e.g., the In-As-In and In-As-Ga pairs. However, the difference is probably within typical experimental error and will be hard to observe. The major interest in this case lies in the third-neighbor peak near $r=4.9$ Å, because the information on the local structures of the first two neighbors can be obtained from the differential PDF's. Each of these four peaks, one in each of (a) and (b) and two in (c) in Fig. 3, consists of two kinds of pairs, e.g., in (a) the peak in In-As curve contains In-As-In-As and In-As-Ga-As pairs, and in (b) the one in Ga-As curve has Ga-As-In-As and Ga-As-Ga-As pairs, etc. These substructures are located so close that they are almost indiscernible even in theoretical calculations. Hence, it will probably not be possible to get information experimentally on the effects of local structure beyond the third-nearest neighbor.

We now discuss the complications on experimental measurements of the differential PDF's imposed by having both a finite q_{max} and a high temperature. The convoluted differential PDF's are shown in Fig. 4 for two different values of q_{max} at a low temperature, where the substructure in the peaks are usually well resolved. Each feature in this substructure in the theoretical calculations is conserved with the higher value of q_{max} in (b), while that associated with the As-related peak for next-nearest neighbor is lost in (a) due to broadening of the peak by the convolution associated with the finite q_{max}. If experiments are done with high enough q_{max} *and* at low enough temperature, one can obtain detailed information on the different types of pairs up to the next-nearest neighbors. The merits of measuring the differential PDF can be noted in Fig. 4(a). Even with $q_{max}=20$ Å^{-1}, the double peak is separated in the differential PDF's for In and Ga. This was not possible in total PDF of Fig. 1(d) with the same experimental conditions.

Another advantage in the differential PDF is that the nearest-neighbor peak positions are not affected by the convolution associated with the finite q_{max}. In the total PDF, on the other hand, the ripples from a nearby peak may change the peak position. For example, consider the nearest-neighbor peak in the As-related curve in (b), which is identical to the total PDF in this case. The peak positions in the double peak from the In-As and the Ga-As pairs interfere with each other to some extent. Also, even with only one measurement of the In-As and Ga-As bond length from the differential PDF, one can deduce the other length with the help of the total PDF. This is because the mean nearest-neighbor distance from the total PDF should be the compositional average of the two. Therefore, the differential PDF can provide a fairly complete description of local structures.

The convoluted differential PDF's for the same two different values of q_{max} as in Fig. 4 are plotted again in Fig. 5. The curves in this figure are calculated at a high temperature where the substructures in the peaks are not resolved in the total PDF. Although we lose the double-peak structure in the As-related curve, which we had in Fig. 4 with $q_{max}=40$ Å^{-1}, the information one can extract remains essentially the same. Therefore, even at a quite high temperature, almost all the advantages of the differential PDF noted in conjunction with Fig. 4 are preserved.

We note that the integrated weights in the various peaks in the partial and differential PDF's are related to the statistical occurrence of pairs of atoms, which we have taken to be given randomly as is appropriate for a random solid solution. For partially ordered alloys, these weights would be different and could be extracted from the integrated intensity in the various peaks.

IV. CONCLUSIONS

We have shown how much more detailed information about the local structure associated with nearest-neighbor and second-neighbor pairs in semiconductor alloys can be obtained from the partial and differential PDF's. Much of this information cannot be extracted from the full PDF. Such information consists of the mean lengths and widths of the various pairs of atoms in the lattice. In addition, if the alloy

is not a random solid solution, this will show up in the integrated weights of the various peaks.

In neutron and x-ray scattering experiments on alloys, there are various problems stemming from convoluting experimental data with a step function, the width of which is determined by the finite value of the maximum momentum transfer. We have shown that this problem is less severe with the partial and differential PDF's than with the total PDF.

ACKNOWLEDGMENTS

We would like to thank S. J. L. Billinge for helpful and stimulating discussions on all aspects of this work. This work was supported by the U.S. Department of Energy under Contract No. DE-FG02-97ER45651. J.S.C. also acknowledges support from the Basic Science Research Institute Program (Contract No. BSRI-97-2436), Korean Ministry of Education.

[1] V. Narayanamurti, Science **235**, 1023 (1987).

[2] J. C. Mikkelsen, Jr. and J. B. Boyce, Phys. Rev. Lett. **49**, 1412 (1982).

[3] J. C. Mikkelsen, Jr. and J. B. Boyce, Phys. Rev. B **28**, 7130 (1983).

[4] S. R. Elliott, *Physics of Amorphous Materials* (Longman, London, 1990); B. E. Warren, *X-ray Diffraction* (Addison-Wesley, Reading, 1969); G. S. Cargill III, in *Solid State Physics*, Vol. 30, edited by H. Ehrenreich, F. Seitz, and D. Turnbull (Academic, New York, 1975); T. Egami, Mater. Trans., JIM **31**, 163 (1990).

[5] J. S. Chung and M. F. Thorpe, Phys. Rev. B **55**, 1545 (1997).

[6] Y. Cai and M. F. Thorpe, Phys. Rev. B **46**, 15 872 (1992); Y. Cai and M. F. Thorpe, *ibid.* **46**, 15 879 (1992); N. Mousseau and M. F. Thorpe, *ibid.* **46**, 15 887 (1992); R. W. Wang, M. F. Thorpe, and N. Mousseau, *ibid.* **52**, 17 191 (1992).

[7] J. S. Chung, M. F. Thorpe, F. Mohiuddin-Jacob, and S. J. L. Billinge, in *Local Structure from Diffraction*, edited by S. J. L. Billinge and M. F. Thorpe (Plenum, New York, 1998), p. 157.

[8] See, for example, *Local Structure from Diffraction*, edited by S. J. L. Billinge and M. F. Thorpe (Plenum, New York, 1998).

[9] J. G. Kirkwood, J. Chem. Phys. **7**, 506 (1939).

[10] M. F. Thorpe, W. Jin, and S. D. Mahanti, in *Disorder in Condensed Matter Physics*, edited by J. A. Blackman and J. Taguena (Oxford University Press, New York, 1991), p. 22.